J. Fluid Mech. (2004), *vol.* 505, *pp.* 225–233.
DOI: 10.1017/S0022112004008547 Printed in the United Kingdom

Solitary wave runup and force on a vertical barrier

By PHILIP L.-F. LIU AND KHALED AL-BANAA

School of Civil and Environmental Engineering, Cornell University, Ithaca, NY 14853, USA

(Received 16 October 2003 and in revised form 9 February 2004)

In this paper we investigate the interaction between a solitary wave and a thin vertical barrier. A set of laboratory experiments was performed with different values of incident wave height to water depth ratio, H/h, and the draught of the barrier to water depth ratio, D/h. While wave gauges were used to measure the reflected and transmitted waves, pressure transducers were installed on both sides of the barrier, enabling the calculation of wave force. The particle image velocimetry (PIV) technique is also employed to measure the velocity field in the vicinity of the barrier. A numerical model, based on the Reynolds-averaged Navier–Stokes (RANS) equations and the k–ϵ turbulence closure model, was first checked with experimental data and then employed to obtain additional results for the range of parameters where the laboratory experiments were not performed. Using both experimental data and numerical results, formulae for the maximum runup height, and the maximum wave force are derived in terms of H/h and D/h.

1. Introduction

For decades wave barriers have been employed as cost-effective structures to protect harbours and marinas from destructive waves. A common type of barrier designed for this purpose is a thin, rigid vertical barrier that extends to some distance below the water surface. This type of barrier allows sediment movements and water exchanges, and reduces the wave energy inside a harbour or a marina. Much theoretical and experimental research have been performed to evaluate the efficiency of vertical wave barriers in terms of transmission and reflection coefficients (e.g. Ursell 1947; Wiegel 1960; Liu & Abbaspour 1982; Losada, Losada & Roldan 1992; Kriebel, Sollitt & Gerken 1998). However, these existing investigations only considered periodic waves and most of them did not account for the energy loss due to flow separation at the tip of the barrier. Furthermore, very little information has been reported on wave forces acting on the barrier, which is an important element in its design.

In the present paper, while we focus on the estimation of the runup height and the maximum force induced by a solitary wave on a vertical wave barrier, we also demonstrate the flow separation patterns and the associated turbulent kinetic energy (TKE) behind the barrier. In a series of laboratory experiments, the reflected and transmitted waves are measured by using wave gauges and the pressure distributions on the barrier are also measured to calculate the force. Furthermore, the particle image velocimetry (PIV) technique is employed to measure the velocity field in the vicinity of the barrier. To consider a wider range of physical parameters than those available from in the experimental set-up, a computational model, based on the Reynolds-averaged Navier–Stokes (RANS) equations (Lin & Liu 1998*a*, *b*), is

Case	A	B	C	D	E	F	G	H
h(m)	0.110	0.125	0.150	0.155	0.185	0.200	0.185	0.185
$Fr = H/h$	0.31	0.08	0.42	0.10	0.05	0.11	0.19	0.34
D/h	0.56	0.60	0.68	0.68	0.75	0.75	0.75	0.75
$\overline{H}/h$	0.50	0.10	0.81	0.13	0.06	0.16	0.31	0.59
F_m/F_o	0.413	0.047	0.840	0.086	0.035	0.156	0.350	0.67
Re	30 818	7 530	77 951	14 908	9 969	26 502	44 512	308 080

TABLE 1. Experimental conditions, wave parameters and measurements.

employed. The results obtained from the computational model are first tested with the experimental data. Very good agreement is observed. Additional numerical results are then obtained for the parameter range not covered by the laboratory experiment. Based on the experimental data and numerical results, formulae for the maximum runup height and maximum wave force are obtained in terms of the incident wave height, H, water depth, h, and the draught of the vertical wave barrier, D.

2. The experiments

The experiments were conducted in a glass-walled wave tank, which is 32 m long, 0.60 m wide, and 0.90 m deep. A rigid thin barrier, with a thickness of 1.8 cm, was installed vertically with an adjustable draught at a distance of 12.5 m downstream from the wavemaker. A piston-type wave generator is used to generate solitary waves with different wave height to water depth ratio, H/h. Table 1 lists the set of parameters, D/h and H/h, used in the experiments. In the same table the measured maximum runup on the barrier, $\overline{H}/h$, and the normalized maximum force, F_m/F_o, in which $F_o = \rho g h^2/2$, are also reported. Note that no breaking wave situation is considered. Capacitance wave gauges are employed to measure wave heights in front and behind the barrier. Eight pressure transducers, OMEGA PX26 pressure sensors with a maximum output of 10 mV, are installed on the front and back face of the barrier. The data sampling rate for both wave gauges and pressure tranceducers is 100 Hz. PIV is employed to measure the velocity field. The details of the PIV system used in the present experiments can be found in Al-Banaa (2000). The field of view (FOV) for the experiments is 18 cm by 18 cm and is placed at the downstream edge of the barrier and just above the bottom of the wave flume. Each experiment is repeated 100 times and the ensemble-averaged velocity field and the turbulent kinetic energy (TKE) are calculated.

Using the dimensional analysis, the maximum force F_m can be expressed as

$$F_m = \phi(\rho, g, h, H, D, \nu), \tag{2.1}$$

which can be regrouped into the following dimensionless form:

$$F_m/F_o = \psi(Fr, D/h, Re). \tag{2.2}$$

The Froude number, Fr, and the Reynolds number, Re, of the physical processes can be defined as

$$Fr = U/\sqrt{gh} = H/h, \qquad Re = UL/\nu = (H/h)(H/h + D/h)g^{1/2}h^{3/2}/\nu, \tag{2.3}$$

in which ν is the kinematic viscosity of the fluid. The characteristic velocity, U, and the lengthscale, L, have been specified as $U = (H/h)\sqrt{gh}$, and $L = (H + D)$, respectively.

The corresponding values of Froude and Reynolds numbers for the experiments are also listed in table 1. The Reynolds number ranges between 10^3 and 10^5. Within this range, the normalized maximum wave force becomes less sensitive to the variation of the Reynolds numbers. Hence, equation (2.2) becomes

$$F_m/F_o = G(H/h, D/h). \tag{2.4}$$

Similar analysis can be carried out for the normalized maximum runup height on the barrier, $\overline{H}/h$, with the same conclusion that for high Reynolds number flows the normalized maximum runup height is a function of D/h and H/h.

3. The computational model

The computational model, COBRAS, which solves the two-dimensional RANS equations with k–ϵ turbulence closure model, is implemented to simulate the experiments and to extend the range of parameters of interest. The RANS equations for the ensemble-averaged velocity, $\langle u_i \rangle$, and the ensemble-averaged pressure, $\langle p \rangle$, are well-known and can be expressed as

$$\frac{\partial \langle u_i \rangle}{\partial x_i} = 0, \tag{3.1}$$

$$\frac{\partial \langle u_i \rangle}{\partial t} + \langle u_j \rangle \frac{\partial \langle u_i \rangle}{\partial x_j} = -\frac{1}{\rho}\frac{\partial \langle p \rangle}{\partial x_i} + g_i + \frac{1}{\rho}\frac{\partial \langle \tau_{ij} \rangle}{\partial x_j} - \frac{\partial \langle u_i' u_j' \rangle}{\partial x_j}, \tag{3.2}$$

in which $i, j = 1, 2$, and $\langle \tau_{ij} \rangle$ is the viscous stress and $-\rho \langle u_i' u_j' \rangle$ denotes the Reynolds stress due to the turbulent fluctuations. We note that u_i' denotes the ith component of the turbulence velocity and $\langle\ \rangle$ the ensemble average. In COBRAS, the Reynolds stress is modelled by the nonlinear stress–strain relation to allow anisotropic turbulence. In this turbulence model information on the turbulent kinetic energy (TKE), k, and its rate of dissipation, ϵ, are needed. Therefore, balance equations for both k and ϵ are also solved in COBRAS. The detailed expressions for the nonlinear Reynolds stress model as well as the k–ϵ equations are lengthy and can be found in the literature (e.g. Lin & Liu 1998*a*). The two-step projection method is employed to solve the RANS equations, while the volume of fluid (VOF) method is used to track the free surface location. COBRAS has already been tested with experimental data for wave shoaling and breaking in the surf zone (Lin & Liu 1998*a*, *b*) as well as for wave–structure interaction problems, in particular for solitary wave propagation over a submerged rectangular obstacle (Chang, Hsu & Liu 2001).

4. Results and discussion

Although all of the experimental runs have been simulated by the computational model, we only present results for case A with $H/h = 0.31$ and $D/h = 0.56$ as a means of illustrating the physical process. In figure 1(*a*, *b*) the wave gauge data at $x = -8.50$ m (upstream of the barrier) and at $x = 2.50$ m (downstream of the barrier) are compared with numerical results. The agreement for the main wave form is excellent. However, discrepancies exist for the small trailing waves. In figure 2, we show a sequence of snapshots of the measured ensemble-averaged velocity field and the normalized TKE as the solitary wave passes under the vertical barrier. The TKE, defined as $k = (1.33/2)\langle u_i' u_i' \rangle$ and shown by the contour lines, has been normalized by the square of the phase speed of the solitary wave, $c^2 = g(H + h)$. In figure 2,

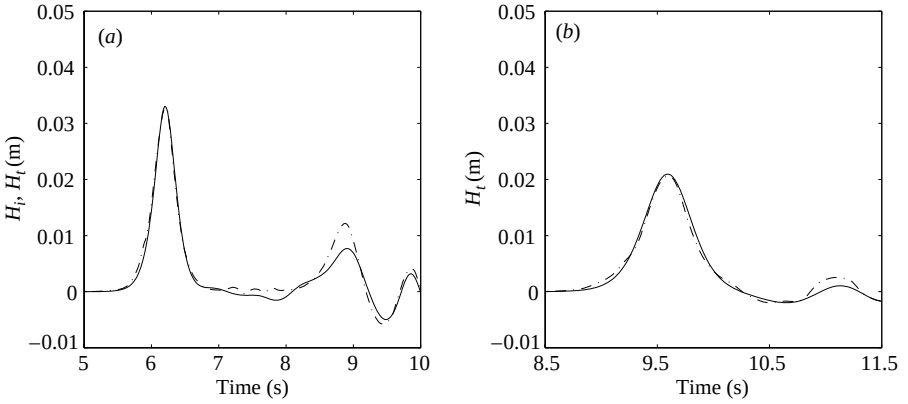

FIGURE 1. Comparisons between the experimental data and numerical results of the time histories of the free surface elevation at two locations for case A: (*a*) incident and reflected waves at $x = -8.50\,\mathrm{m}$; (*b*) transmitted waves at $x = 2.50\,\mathrm{m}$. The dashed line and the solid line correspond to the experimental data and numerical results, respectively.

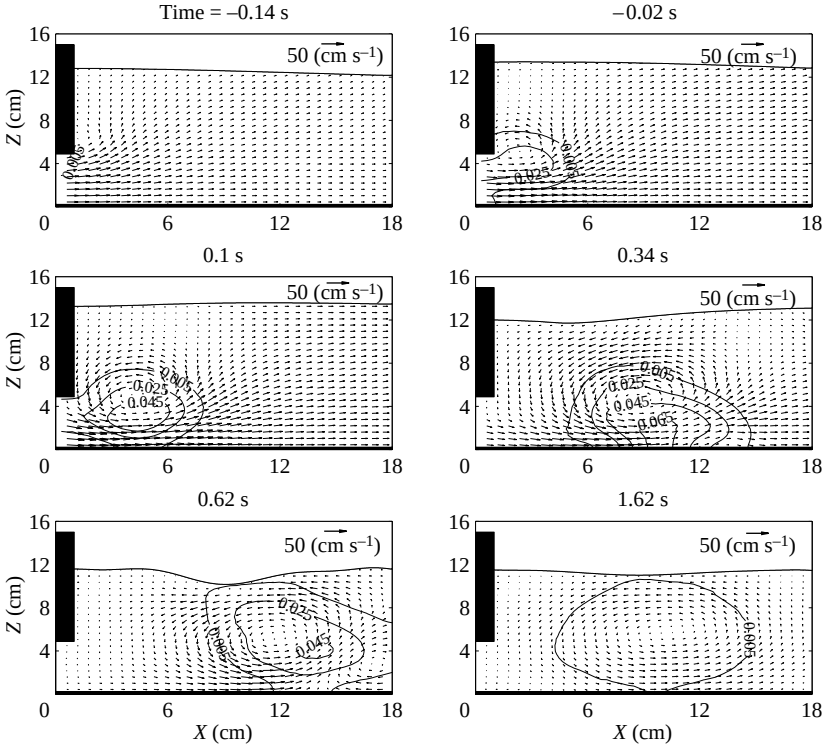

FIGURE 2. Snapshots of the measurements for ensemble-averaged velocities (vectors) and the normalized turbulent kinetic energy (contour lines) as the solitary wave passing the vertical barrier. The TKE is normalized by $c^2 = g(H + h) = 1.42\,\mathrm{m^2\,s^{-2}}$.

the crest of the solitary wave arrives at the barrier at $t = 0$ and the phase speed of the solitary wave for Case A is $1.19\,\mathrm{m\,s^{-1}}$. It is clearly shown that as the wave crest approaches the vertical barrier, flow separation occurs behind the barrier and a large eddy is generated. The eddy is advected downstream with a speed much smaller than

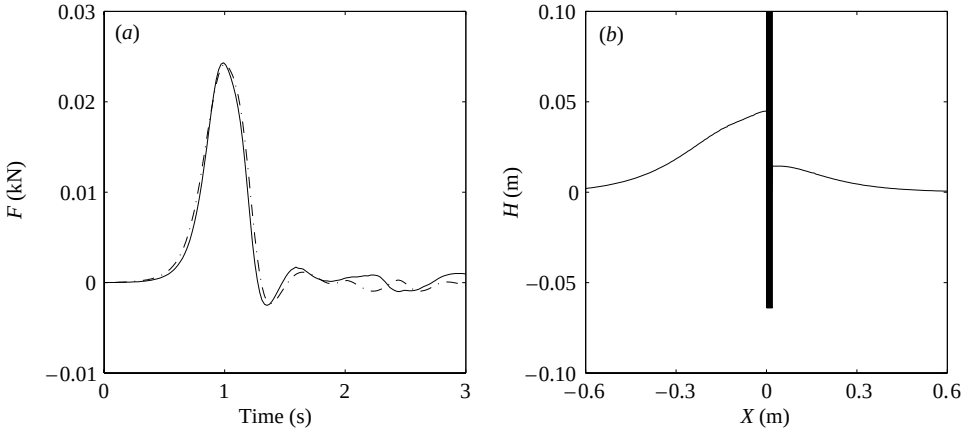

FIGURE 3. (*a*) The comparison between numerical results (solid lines) and experimental data (dashed line) for the wave force acting on the barrier for case A. (*b*) The snapshot of the free surface profile at the moment when the maximum wave force occurs.

the phase speed. At the same time, the eddy diffuses in all direction and reaches the free surface. The intensity of the TKE correlates with the location of the eddy very well and it reaches a maximum value long after the wave crest has propagated downstream from the barrier. Depending on the incident wave height and the draught of the barrier, the TKE could be significant. In Case A, the maximum TKE value is about 6% of the square of the phase speed and, hence, the maximum turbulence velocity is about 30% of the corresponding ensemble-averaged velocity (see the panel for time = 0.34 s). Calculating the kinetic and potential energy associated with the incident, reflected, and transmitted waves, respectively, we estimate that in case A the total energy of the reflected wave is about 12.4% of the total energy of the incident wave, while the total energy of the transmitted wave is about 64.7%. Therefore, in this case, about 23% of the incident wave energy is dissipated primarily through the flow separation near the tip of the barrier.

The wave forces acting on the barrier can be determined directly by integrating the measured pressures over the submerged portion of the barrier. Figure 3(*a*) shows the time histories of the force for the case discussed above. Both experimental data and numerical results are plotted together. The agreement is excellent. The free surface profile at the time when the maximum positive force occurs is shown in figure 3(*b*). The maximum force occurs slightly before the runup on the front side of the barrier reaches the maximum runup height, $\overline{H}$. To further ensure that the numerical solutions are accurate, the incident wave heights and the maximum wave forces obtained from experiments and numerical simulations are plotted against each other in figures 4(*a*) and 4(*b*), respectively for all the cases listed in table 1. The agreement is again excellent. Therefore, we have confidence in using the numerical model as a tool to further explore the problem with a wider range of parameters.

One of the important design consideration for a vertical barrier is the maximum runup height, $\overline{H}$. To find the relationship among, $\overline{H}/h$, H/h, and D/h, we have performed 67 numerical simulations for $0 \leqslant D/h \leqslant 1.0$ and $0.032 \leqslant H/h \leqslant 0.42$. The corresponding Reynolds numbers vary from 560 to 6.27×10^6. It is important to point out that simulations were also performed for the prototype scale to ensure that the scaling effects are not important. Using the experimental data as well as the numerical

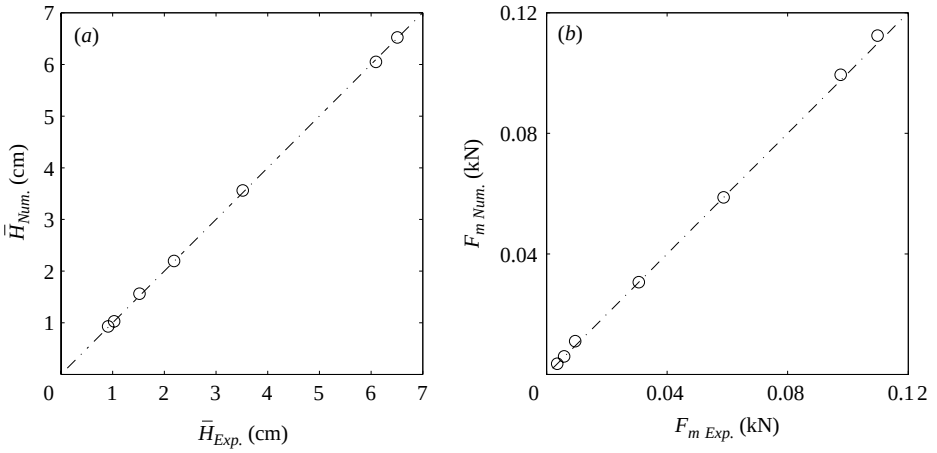

FIGURE 4. Direct comparison of the experimental and numerical results for (*a*) maximum runup height for all the cases tabulated in table 1, and (*b*) maximum wave forces (dot-dashed line is 45° straight line).

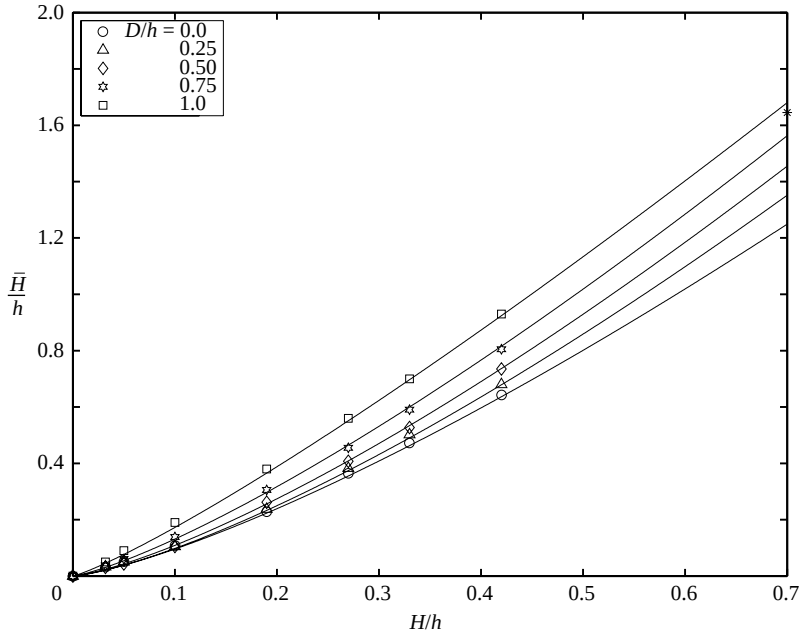

FIGURE 5. The maximum runup, $\overline{H}/h$, at the barrier as a function of H/h and D/h. The solid lines represent the suggested equation (4.1), and the symbols denote different D/h values.

results, we found the following relationship:

$$\overline{H}/h = \alpha(H/h)^{\beta}, \tag{4.1}$$

where

$$\alpha = 2.0 + 0.81(D/h) - 0.26(D/h)^2, \qquad \beta = 1.32 + 0.20(D/h) - 0.35(D/h)^2. \tag{4.2}$$

In figure 5, equation (4.1) with (4.2) is plotted for $\overline{H}/h$ in terms of D/h and H/h. It is clear that the maximum runup height increase as the incident wave height and

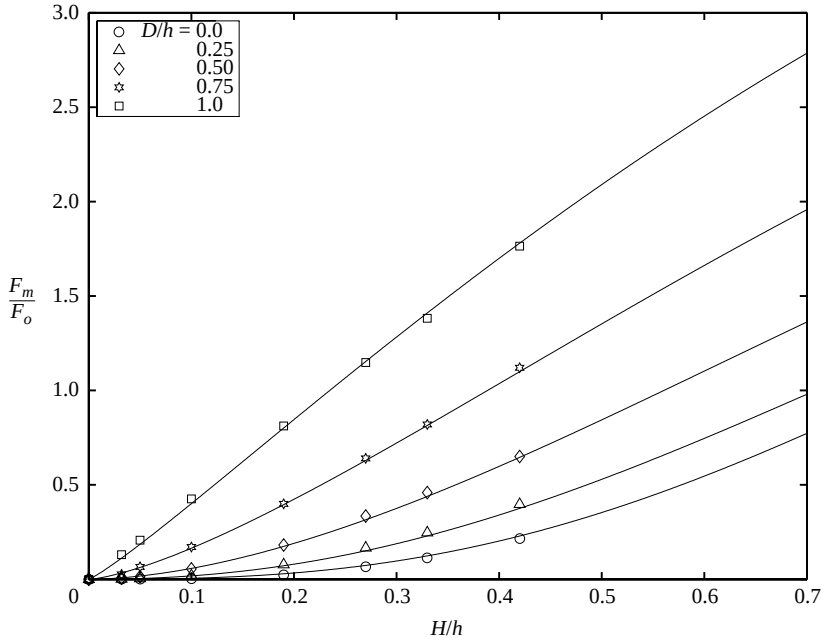

FIGURE 6. The maximum wave force, F_m/F_o, as a function of H/h and D/h. The solid lines denote the suggested equation (4.6) and the symbols denote different D/h values.

the draught increase. When $D = h$, i.e. the vertical barrier is completely down, the incident wave is completely reflected. Equation (4.1) becomes

$$\overline{H}/h = 2.55(H/h)^{1.17}. \tag{4.3}$$

The analytical solutions by Byatt-Smith (1971) and the experimental observations of Maxworthy (1976) have shown that the maximum runup, $\overline{H}$, can be approximated as

$$\overline{H}/h = 2.0(H/h) + 0.5(H/h)^2. \tag{4.4}$$

The differences between equation (4.3) and (4.4) are very small for $0 \leqslant H/h \leqslant 0.7$. The maximum difference is only about 2% at $H/h = 0.7$. When $D/h = 0$, the maximum runup becomes

$$\overline{H}/h = 2.0(H/h)^{1.32}, \tag{4.5}$$

When the wave amplitude and draught ratios are moderate, $H/h \leqslant 0.3$ and $D/h \leqslant 0.25$, equation (4.5) can be used as an approximation of the maximum wave runup $\overline{H}/h$.

Using all the experimental data and the numerical results for the maximum force, the following dimensionless formula can be obtained:

$$F_m/F_o = \delta\{1 - \exp[-(H/h)^{\gamma}]\}, \tag{4.6}$$

where

$$\delta = 2.4 + 0.22(D/h) + 3.11(D/h)^2, \qquad \gamma = 2.65 - 2.08(D/h) + 0.57(D/h)^2. \tag{4.7}$$

Equation (4.6) is plotted in figure 6. Overall, the effects of nonlinearity, H/h, are much more important when D/h is larger. When $D = h$, i.e. the vertical barrier is

completely down, equation (4.6) becomes

$$F_m/F_o = 5.73\{1 - \exp[-(H/h)^{1.14}]\}. \tag{4.8}$$

The above equation is similar to that presented by Cooker, Weidman & Bale (1997), and further approximation by expanding the exponential to the leading-order approximation for small H/h, i.e. $H/h \leqslant 0.20$, and using equation (4.3), leads to equation (4.8) becoming a linear function of $\overline{H}/h$, which can expressed as

$$F_m/F_o = 2.17(\overline{H}/h). \tag{4.9}$$

On the other hand, when $D/h = 0$, equation (4.6) becomes

$$F_m/F_o = 2.40\{1 - \exp[-(H/h)^{2.65}]\}. \tag{4.10}$$

The maximum wave force can be rescaled by the hydrostatic force on the vertical barrier using the maximum runup height, i.e. $\frac{1}{2}\rho g\overline{H}^2$. For a small incident wave height, the leading-order maximum wave force can be expressed as

$$F_m \approx 0.60\left(\tfrac{1}{2}\rho g\overline{H}^2\right). \tag{4.11}$$

The scaled maximum wave force is independent of $\overline{H}/h$ (or H/h) for small values of H/h. Thus, the maximum wave force is roughly 60% of the hydrostatic force in terms of the maximum runup height $\overline{H}/h$ at the vertical barrier.

5. Concluding remarks

Based on the experimental data as well as the numerical results, we have derived two useful formulae for estimating the maximum solitary wave runup height and the maximum force on a vertical barrier. These formulae are expressed in terms of incident wave height to depth ratio, H/h, and the draught to depth ratio, D/h. They are valid for non-breaking solitary waves. These formulae should be useful in designing such wave barriers. During the experiments reported here, velocity field data were also taken by using the PIV technique. Flow separation and vortex generation were clearly observed (see figure 2). The turbulent kinetic energy associated with the vortex can be very significant. The detailed analysis of the flow field and the comparisons between experimental data and numerical results will be reported elsewhere. New laboratory and numerical experiments are being carried out for the periodic incident wave case.

The authors wish to acknowledge Kuwait Institute for Scientific Research (KISR) for providing financial support for K. Al-Banaa and the US National Science Foundation for the research grants to Cornell University. We would also like to thank Dr Cliff Astill, director of Geo-Hazard program at the National Science Foundation, for his continuous support.

REFERENCES

Al-Banaa, K. A. A. 2000 Experimental study of the bottom boundary layer induced by water waves propagation over a rippled bed. Master thesis, Cornell University.

Byatt-Smith, J. G. B. 1971 An integral equation for unsteady surface waves and a comment on the Boussinesq equation. *J Fluid Mech.* **49**, 625–633.

Chang, K. A., Hsu, T. J. & Liu, P. L.-F. 2001 Vortex generation and evolution in water waves propagating over a submerged rectangular obstacle, part I. solitary waves. *Coastal Engng* **44**, 13–36.

Cooker, M. J., Weidman, X. & Bale, D. S. 1997 Reflection of a high-amplitude solitary wave at a vertical wall. *J Fluid Mech.* **342**, 141–158.

Kriebel, D., Sollitt, C. & Gerken, W. 1998 Wave forces on a vertical wave barrier. *Proc. 26th Intl Conf. Coastal Engng, ASCE* (ed. B. L. Edge), pp. 2069–2483.

Lin, P. & Liu, P. L.-F. 1998*a* A numerical study of breaking waves in the surf zone. *J. Fluid Mech.* **359**, 239–264.

Lin, P. & Liu, P. L.-F. 1998*b* Turbulent transport, vorticity dynamics and solute mixing under plunging breaking waves in surf zone. *J. Geophys. Res.* C **103**, 15677–15694.

Liu, P. L.-F. & Abbaspour, M. 1982 Wave scattering by a rigid thin barrier. *J. Waterway, Port, Coastal Ocean Div., ASCE* **108**, 479–491.

Losada, I. J., Losada, M. A. & Roldan, A. J. 1992 Propagation of oblique incident waves past rigid vertical thin barriers. *Appl. Ocean Res.* **14**, 191–199.

Maxworthy, T. 1976 Experiments on the collision between two solitary waves. *J Fluid Mech.* **76**, 177–185.

Ursell, F. 1947 The effect of a fixed barrier on surface waves in deep water. *Proc. Camb. Phil. Soc.* **43**, 374–382.

Wiegel, R. 1960 Transmission of waves past a rigid vertical thin barrier, *J. Waterways Harbors Div., ASCE* **86**, 1–12.